Mechanical Systems and Signal Processing 141 (2020) 106506

Contents lists available at ScienceDirect

Mechanical Systems and Signal Processing

journal homepage: www.elsevier.com/locate/ymssp

Bayesian identification of electromechanical properties in piezoelectric energy harvesters

Patricio Peralta [a,c], Rafael O. Ruiz [b,c,*], Alexandros A. Taflanidis [d,e]

[a] Department of Mechanical Engineering, Universidad de Chile, Chile
[b] Department of Civil Engineering, Universidad de Chile, Chile
[c] Uncertainty Quantification Group, Center for Modern Computational Engineering, Universidad de Chile, Chile
[d] Department of Civil & Environmental Engineering & Earth Sciences, University of Notre Dame, USA
[e] Department of Aerospace and Mechanical Engineering, University of Notre Dame, USA

ARTICLE INFO

Article history:
Received 31 May 2019
Received in revised form 21 October 2019
Accepted 6 November 2019
Available online 9 January 2020

Keywords:
Bayesian model updating
Piezoelectric Energy Harvesters
Model class selection
Model prediction error
Electro-mechanical properties identification

ABSTRACT

The model updating of the electro-mechanical properties of Piezoelectric Energy Harvesters (PEHs) using experimental data within a Bayesian inference setting is discussed. The implementation requires: a predictive model for the harvester response; an assumption for its prediction error; a prior multivariate probabilistic density function for the electromechanical properties; and experimental measurements of the harvester response. Different approaches are compared with respect to the Bayesian model updating, including point estimates of the updated properties based on Maximum a Posteriori and Maximum Likelihood Estimates, as well as a full description of the posterior density for the model characteristics, obtained through a Transitional Markov Chain Monte Carlo approach. A model class selection implementation is also discussed that allows for the consideration of some PEH properties as either deterministic or aleatoric (uncertain) variables. The overall framework offers an elegant approach to calibrate PEH numerical/analytical model or identify variability trends for the PEH manufacturing process.

1. Introduction

The use of piezoelectric energy harvesters (PEHs) to feed low-power electronics has been widely studied in the last decade, with one (but not the only) prominent application being the development of low-cost remote sensing technologies. The most common configuration of PEHs consists of a cantilevered plate composed of a series of intercalated piezoelectric layers. These layers are connected by an elastic material that serves as a support structure, enforcing strains that are transformed to electric charge by the piezoelectric material. When PEHs employ two piezoelectric layers bonded to a central support sheet, they are referenced as bimorph PEHs (also shown in Fig. 1). These (two) layers could be connected in series or parallel configuration depending whether the goal is to increase the output voltage or current, respectively.

Noteworthy efforts have been made in the past to describe the dynamic behavior of these devices. In particular, the model proposed by Erturk and Inman [1–3] has received significant attention, since it properly formulates the coupled electromechanical problem while offering a tractable analytic solutions based on a Bernoulli-beam theory. Beyond this seminal work, other models have been proposed, using finite elements principles [4], linear and nonlinear distributed parametric

* Corresponding author at: Department of Civil Engineering, Universidad de Chile, Chile.
E-mail address: rafaelruiz@uchile.cl (R.O. Ruiz).

https://doi.org/10.1016/j.ymssp.2019.106506
0888-3270/

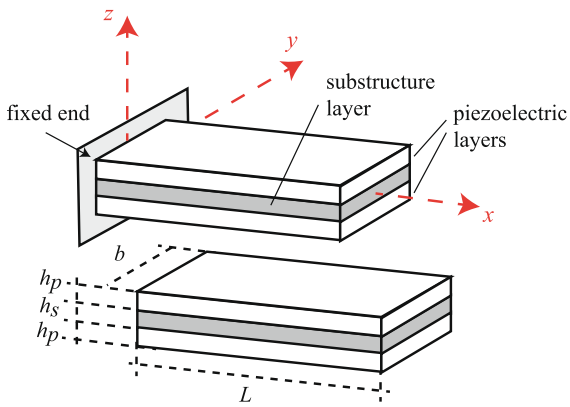

Fig. 1. Typical scheme of a rectangular Bimorph PEH in a cantilevered condition. Substructure and piezoelectric layers are also shown together with the main geometrical parameters.

modeling [5–8], or isogeometric analysis [9]. These approaches provide an increased degree of complexity for the PEH model, allowing the consideration of nonrectangular geometries, large deformations and nonlinear piezoelectric effects.

All modeling efforts discussed in the previous paragraphs offer deterministic predictions, with accuracy that may be compromised when the knowledge about their model characteristics is not complete. In practical applications, though, uncertainties, typically related to the lack of information about the exact value of the PEH device electromechanical properties and geometrical characteristics, are expected to exist. For example, Kim et al. [10] identified that small variations in the tip mass position of micro-PEHs induces a significant variation in the dynamic predictions. Similar results were obtained by Ruiz and Meruane [11] in macro-PEHs, using a global sensitivity analysis that revealed that the tip mass position, the imperfect clamping condition of the harvester, and certain electromechanical properties are responsible for largest portion of the variations observed for the frequency response function (FRF) of the device. Motivated by such realizations, different authors have proposed methodologies based on stochastic sampling techniques to propagate the uncertainties associated with the PEH model parameters, assuming as uncertain either all parameters [11,12] or only a smaller subset [13,14]. The uncertainty propagation in these studies has helped quantify the potential impact of modeling uncertainties on the predicted response of PEHs. For example, in [11] and using typical variation of electromechanical properties compared to their nominal values, it was shown that the predicted fundamental frequency of the harvester has a coefficient of variation close to 10%, while the probability that the peak FRF amplitude will be higher than the nominal prediction is <10%. Similar conclusions have been drawn in other studies [15,16].

This variability in the predicted FRF provides an important challenge, since the likelihood that the manufacturer will provide a device with the desirable FRF characteristics (within some tolerance bounds) might be small. To address this challenge, different optimization strategies have been recently proposed considering parametric uncertainty in the PEH model description. In [17] the optimization of PEH devices was examined using as objective function the worst-case electrical power generation performance under the possible uncertainties associated with the natural frequency, the load resistance and the electromechanical coupling coefficient of the device. Instead of focusing on the worst anticipated performance, a probabilistic formulation was discussed in [18], establishing a design methodology that guarantees a specific reliability for the electrical power, while considering uncertainties associated with the length, the tip mass, and the electromechanical properties of the PEH.

Although different techniques have been established to propagate the uncertainties associated with the PEH model characteristics and ultimately to design PEHs considering such uncertainties, the identification of the model parameters of a particular device, including the characterization of the uncertainty in this identification, remains an open question. For example, in the recent study by Peralta et al. [12] that experimentally identified the FRFs of 20 nominally identical bimorph PEHs, it was shown that the estimated FRFs significantly differed from the expected ones corresponding to the nominal device characteristics. The same study identified the electro-mechanical properties (rather than the geometrical characteristics) of the PEHs as the most important source of the observed variability. Since the geometrical characteristics of a PEH can be estimated with adequate accuracy using instruments like micrometers or calipers, the aforementioned observation poses the important question of how to infer the electromechanical properties of the harvester once the experimental FRF and the geometrical parameters are known. Note that the FRF can be also measured with reasonable precision using, for example, the experimental procedure discussed in [12].

Traditional strategies to identify (infer) parameters of mechanical system models using observation data rely on minimizing, with respect to these parameters, the discrepancy (expressed typically as the squared error) between the experimental observations and the model predictions [19]. Such approaches provide a deterministic estimate to represent the actual value of the model parameter of interest, and therefore a deterministic predictive system model. There exist, though, alternative strategies grounded in a probability logic foundation, mainly methods based on Bayesian inference [20] (also referenced as

Bayesian updating), which explicitly account for uncertainties associated with the parameter identification process. The implementation of Bayesian inference to PEHs is particularly attractive due to the relevance, discussed in the previous paragraph, of the PEH model parameter variability in the predicted response. Bayesian inference starts with a probabilistic definition of the initial knowledge about the model parameter variability, quantified though a probability density function (PDF), which in this context is called the prior PDF. Utilizing the experimentally observed data it proceeds to update this prior PDF to obtain the posterior PDF for the model parameters, expressed by Bayes' theorem though the prior PDF and the likelihood of the observed data. Estimation of the posterior PDF represents, though, a challenging task; it can be approximated though samples generated by some advanced stochastic simulation method, for example Markov Chain Monte Carlo (MCMC) [21], or it can be approximated focusing on its peak(s) (maximum of posterior PDF) [22], typically referenced as Maximum a Posteriori or MAP parameters. In the former case full information about the uncertainty for the posterior parameter distribution is obtained whereas in the latter case statistics can be obtained as point estimates [23]. Parenthetically, note that the popular Maximum Likelihood Estimate (MLE) parameter identification [24] can be interpreted as a particular instance of Bayesian inference MAP estimation, one corresponding to a uniform prior PDF [20]. It should pointed out that beyond Bayesian inference, other non-probabilistic formulations exist for considering uncertainties in model updating, adopting, for example, interval analysis to account for the variability associated with model parameters by the introduction of boundary rules [25–28].

The uncertainty quantification facilitated through the identification of the posterior PDF within a Bayesian updating scheme is, furthermore, compatible with existing frameworks for uncertainty propagation in PEHs [11,12]; in this context the use of the initial (prior) or the updated (posterior) PDFs provide, respectively, the prior and posterior predictive models, facilitating ultimately a robust to uncertainties predictive analysis. For PEHs implementation this pertains to the output variability, whereas the updated predictions, with hopefully a decreased level of uncertainty, are facilitated through new information obtained through the experimentally identified FRFs. Beyond the parameter identification, the Bayesian updating scheme can furthermore support the selection of the most probable model among a class of candidate models, what is formally defined as model class selection. In this case the experimental observations are used to update the relative plausibility of each of the considered models [22]. Notably this model class selection approach automatically enforces a principle of model parsimony, balancing between data fit and model complexity.

For PEH applications the Bayesian updating paradigm is very promising since it allows to both select the most appropriate model for a specific energy harvesting application, as well as the set of model parameters that should be considered in forming the predictions based on that model. In this context, the objective of this work, and the main novel contribution, is the implementation of Bayesian inference techniques to PEHs. Theoretical details related to the adoption of Bayesian techniques for the identification of the electromechanical properties of PEHs are first reviewed to offer the reader with a complete foundational background, and subsequently emphasis is placed on computational/numerical details related to the most appropriate method to identify the posterior PDF for this specific application as well as to the implementation of model class selection to identify which PEH properties could be considered as deterministic. This ultimately establishes a framework to: (1) identify the actual characteristic of PEHs, and (2) select the most appropriate PEH model. Though the theoretical and computational foundation of this Bayesian framework has been previously developed, its application to PEH, including investigation of the appropriateness of different numerical approaches to facilitate the posterior PDF identification, constitutes a powerful tool in the robust design and performance prediction for these devices. The rest of the paper is organized as follows. Section 2 reviews the Bayesian updating and predictive analysis scheme, focusing on essential theoretical and computational aspects that can promote a better understanding for its implementation to PEHs. Section 3 discusses specifics for the PEH implementation. Finally, Section 4 presents the case study for identification of properties of commercial PEHs and discusses in detail the appropriateness for this application of the different techniques reviewed in Section 2.

2. Bayesian inference for model parameter updating and model class selection

2.1. Fundamentals and model parameter updating

To formalize the Bayesian updating problem, let $H(\theta,\omega)\in\mathbb{R}$ denote the output of the system model, where $\theta\in\mathbb{R}^{Np}$ corresponds to the model parameter vector and $\omega\in\mathbb{R}$ to the system input. In the context of the PEH application discussed in this paper, and detailed in Section 3, H corresponds to the frequency response and ω to the excitation frequency. A prediction error e is introduced to account for the discrepancy between model output $H(\boldsymbol{\theta},\omega)$ and actual system output h. Two common approaches for incorporating this error in the analysis are to assume either an additive or multiplicative influence, leading to system output given, respectively, by

$$h = H(\theta,\omega) + e \tag{1}$$

$$h = H(\theta,\omega)\, e \tag{2}$$

Note that for strictly positive outputs (like the FRF) the multiplicative error can be simply treated as an additive error between the logarithms $\ln(h)$ and $\ln(H)$. The prediction error is modeled as an (aleatoric) uncertain parameter, leading, ultimately, to a probabilistic description for h. The additive prediction error is typically modeled as a Gaussian random variable

with zero mean and standard deviation σ_e. More details about the selection of this distribution, including its connection to information theory and the maximum entropy principle can be found in [22]. Under this assumption, the system output h follows a Gaussian distribution with mean $H(\theta,\omega)$ and standard deviation σ_e leading to a PDF (probability density function) for h defined by:

$$p(h|\theta_t,\omega)=\frac{1}{\sigma_e\sqrt{2\pi}}\exp\left[-\frac{1}{2\sigma_e^2}(h-H(\theta,\omega))^2\right] \tag{3}$$

where $\boldsymbol{\theta}_t$ corresponds to the augmented parameter vector needed for definition of the probability distribution for the system output h, composed of both the parameters $\boldsymbol{\theta}$ of the deterministic model $H(.)$ as well as the characteristic for the prediction error, in this case σ_e.

For the multiplicative error case, similar assumptions are utilized for the prediction error, in this case with respect to the logarithm of the respective quantities, since as discussed above multiplicative error is equivalent to additive error with respect to the logarithm of the output. This leads to a lognormal distribution for e and, consequently, for h

$$p(h|\theta_t,\omega)=\frac{1}{h\,\sigma_e\sqrt{2\pi}}\exp\left[-\frac{1}{2\sigma_e^2}(\ln(h)-\ln(H(\theta,\omega)))^2\right] \tag{4}$$

where σ_e is the standard deviation of $\ln(e)$.

Assume, now, that M observations (measurements) are provided for the system output $\left\{\hat{h}_m\,;m=1,\ldots,M\right\}$ for different inputs $\{\hat{\omega}_m;m=1,\ldots,M\}$, obtained through some experimental procedure. Let $\hat{\mathbf{W}}=\{\hat{\omega}_1\cdots\hat{\omega}_M\}$ and $\hat{\mathbf{h}}=\left\{\hat{h}_1\cdots\hat{h}_M\right\}$ denote, respectively, the input and output vectors and $\mathbf{D}$ the experimental data pair composed of both $\hat{\mathbf{W}}$ and $\hat{\mathbf{h}}$. The likelihood of the observations $\hat{\mathbf{h}}$ assuming independence of the errors between them is given by

$$p\left(\hat{\mathbf{h}}\middle|\theta_t,\hat{\mathbf{W}}\right)=\prod_{m=1}^{M}p\left(\hat{h}_m|\theta_t,\hat{\omega}_m\right) \tag{5}$$

For the additive and multiplicative error cases, with predictive models given by Eqs. (3) and (4), respectively, this simplifies to

$$p\left(\hat{\mathbf{h}}\middle|\theta_t,\hat{\mathbf{W}}\right)=\left(\frac{1}{\sigma_e\sqrt{2\pi}}\right)^M\exp\left[-\frac{1}{2\sigma_e^2}\sum_{m=1}^{M}\left(\hat{h}_m-H(\theta,\hat{\omega}_m)\right)^2\right] \tag{6}$$

$$p\left(\hat{\mathbf{h}}\middle|\theta_t,\hat{\mathbf{W}}\right)=\left(\frac{1}{\sigma_e\sqrt{2\pi}}\right)^M\left(\prod_{m=1}^{M}\frac{1}{\hat{h}_m}\right)\exp\left[-\frac{1}{2\sigma_e^2}\sum_{m=1}^{M}\left(\ln\left[\hat{h}_m\right]-\ln[H(\theta,\hat{\omega}_m)]\right)^2\right] \tag{7}$$

If the prior belief of the model parameter θ_t is defined by PDF $p(\theta_t)$ then Bayes Theorem leads to the updated probabilistic description for it using data $\mathbf{D}$

$$p(\theta_t|\mathbf{D})=\frac{p(\mathbf{D}|\,\theta_t)p(\theta_t)}{\int p(\mathbf{D}|\,\theta_t)p(\theta_t)d\theta_t}=\frac{p(\hat{\mathbf{h}}|\,\theta_t,\hat{\mathbf{W}})p(\theta_t)}{P(\hat{\mathbf{h}}|\hat{\mathbf{W}})} \tag{8}$$

Distribution $p(\theta_t|\mathbf{D})$ is called the posterior PDF, and it reads as the PDF of θ_t given the experimental data $\mathbf{D}$. The denominator in Eq. (8) is simply a normalizing constant for the PDF and is also called the evidence of the system [29]. An important note here is that the measurement errors are assumed negligible compared to the prediction errors; if not, then Eq. (3) [or Eq. (4)] should be modified to include them, assuming an appropriate probabilistic model for the measurement noise.

Ultimately, the identification of the updated distribution $p(\theta_t|\mathbf{D})$ is the fundamental objective of the Bayesian inference scheme as it facilitates a robust approach to calibrate the PEHs model parameters, including an explicit quantification of the associated uncertainties which can be further utilized to provide robust predictions using the updated system model. As will be discussed in Section 2.4. This identification further facilitates model comparisons that explicitly balances between model accuracy and model complexity.

Characterization of the $p(\theta_t|\mathbf{D})$ and predictions using the updated probabilistic system characterization can be established either by approximating distribution $p(\theta_t|\mathbf{D})$ by a point estimate, corresponding to the most probable value for θ_t, or by utilizing the entire distribution $p(\theta_t|\mathbf{D})$, typically through samples from it [21]. These choices are discussed next.

2.2. Point estimates: maximum a posteriori (MAP) and maximum likelihood estimate (MLE)

The most representative value of θ_t given the observation data $\mathbf{D}$, corresponds to the peak (maximum) of the posterior PDF $p(\theta_t|\mathbf{D})$, leading to the MAP (maximum a posteriori) estimate [20]:

$$\theta_t^{MAP}=\arg\max\left[\ln\left(p(\hat{\mathbf{h}}|\,\theta_t,\hat{\mathbf{W}})p(\theta_t)\right)\right] \tag{9}$$

where logarithm was introduced in the maximization of Eq. (9) simply for numerical convenience [20]. The values identified in Eq. (9) correspond to the peak of the $p(\theta_t|\mathbf{D})$ (note that the denominator in Eq. (8) is merely a constant and therefore does not impact optimization). This optimization is also related to the popular Maximum Likelihood Estimate (MLE) [30] which focuses simply on maximization of the likelihood function $p(\hat{\mathbf{h}}\big|\,\theta_t,\hat{\mathbf{W}})$ without using any prior information for the system model

$$\theta_t^{MLE} = \arg\max\left[\ln\left(p(\hat{\mathbf{h}}\big|\,\theta_t,\hat{\mathbf{W}})\right)\right] \tag{10}$$

For a Gaussian assumption for the model prediction error, as is the case discussed Section 2.1 for Eqs. (6) and (7), the MLE parameter estimate in Eq. (10) corresponds to a least-squares estimate [31]. In this context the MAP estimate can be regarded as a generalized least-squares estimate with an added regularization term, stemming from the prior information $p(\theta_t)$ [30].

The optimizations in Eqs. (9) and (10) may have a single optimum, multiple, discrete local optima or a continuous manifold (in θ_t space) of equally likely solutions. The system is characterized respectively as globally identifiable, locally identifiable or unidentifiable [22]. For large data set (large number of experiments M) it is expected that the MAP and MLE model parameters converge, as the information provided through the observations $p(\hat{\mathbf{h}}\big|\,\theta_t,\hat{\mathbf{W}})$ eventually outweighs the prior information incorporated through $p(\theta_t)$.

Ultimately, MAP (or MLE in simplified form) provides a representation of the posterior PDF $p(\theta_t|\mathbf{D})$ though a single point (or multiple points in case of a not globally identifiable system). Statistics related to this PDF can be obtained by adopting Laplace's method of asymptotic approximation [32] as will be discussed later, an approach that provides accurate result as long as the likelihood function is peaked, a condition typically satisfied for large M for globally identifiable systems. This property ultimately makes expansions that concentrate solely at a single point (the peak of the posterior), rather than the entire support of $p(\theta_t|\mathbf{D})$,valid [22,30] since the integrand is highly concentrated in these regions. Since prior distributions are expected to be relatively flat, this behavior (high sensitivity of posterior) can be established only through the influence of the likelihood function. Furthermore, in such instances the distribution $p(\theta_t|\mathbf{D})$ itself can be reasonably approximated [23,22] as a Gaussian, centered at θ_t^{MAP} with covariance matrix corresponding to the inverse of Hessian

$$\mathbf{H}_s(\theta_t) = -\nabla_{\theta_t}\nabla_{\theta_t}\ln\left(p(\hat{\mathbf{h}}\big|\,\theta_t,\hat{\mathbf{W}})p(\theta_t)\right) \tag{11}$$

evaluated at θ_t^{MAP}, $\mathbf{H}_s(\theta_t^{MAP})$. If λ is the minimum eigenvalue of $\mathbf{H}_s(\theta_t^{MAP})$ then $1/\sqrt{\lambda}$ represents the largest spread (curvature) of the integrand around each of its principal directions [eigenvectors of $\mathbf{H}_s(\theta_t^{MAP})$] and is an indication of how appropriate the point estimate approximation is [33]. Small spread (small curvature) indicates a concentration of the posterior around a single point and increase the accuracy of the approximation. Of course if the posterior $p(\theta_t|\mathbf{D})$ is indeed a Gaussian, then the fit with a Gaussian distribution is an accurate one (same applies to accuracy of Laplace's expansion), independent of the value of λ.

This approximation of the posterior PDF $p(\theta_t|\mathbf{D})$ and resultant statistics utilizing only a point estimate might be inappropriate when that PDF has a more complex form. In such instances the entire PDF $p(\theta_t|\mathbf{D})$ needs to be taken into account, something typically done through stochastic sampling approaches that provide samples of θ_t from that distribution [22]. Approaches to perform this task typically rely on MCMC (Markov Chain Monte Carlo) sampling. The Transitional Markov Chain Monte Carlo (TMCMC) method [34,35], an approach employed in multiple similar applications [36–38] and the one utilized in the illustrative example considered later in this paper, is reviewed next for this purpose. It is important to stress that there exist a number of alternative methods for the posterior PDF approximation, for example approaches that combine importance sampling and tempering techniques [39–43]. Any of these techniques could have been used here in place of TMCMC.

2.3. Sampling from $p(\theta_t|\mathbf{D})$ and Transitional Markov Chain Monte Carlo

Foundation of TMCMC is a sequential implementation using a series of intermediate auxiliary PDFs (also known as tempered densities) to converge to the posterior PDF $p(\theta_t|\mathbf{D})$ starting from the prior PDF $p(\theta_t)$ [34,35]. These auxiliary densities $\{p_j(\theta_t|\mathbf{D}) : j = 0,\ldots,n\}$ are defined following the proportional relationship shown in Eq. (8) as $p_j(\theta_t|\mathbf{D}) \propto p(\hat{\mathbf{h}}\big|\,\theta_t,\hat{\mathbf{W}})^{q_j}p(\theta_t)$, with the transition from one density to the other controlled by the exponent $q_j \in [0,1]$. For the two extremes, $q_0 = 0$ and $q_n = 1$, the densities correspond, respectively, to $p_0(\theta_t|\mathbf{D}) \propto p(\theta_t)$ [prior] and $p_n(\theta_t|\mathbf{D}) \propto p(\theta_t|\mathbf{D})$ [posterior], with the intermediate densities used to facilitate the move from the known prior to the unknown, and difficult to sample from, posterior. The sequence of intermediate densities is utilized to simply make the latter sampling easier; by carefully selecting the sequence $\{q_j : j = 1,\ldots,n-1\}$, the difference between subsequent densities $p_j(\theta_t|\mathbf{D})$ and $p_{j+1}(\theta_t|\mathbf{D})$ is kept small, so that the former can provide sufficient information to guide sampling from the latter. This is established using a resampling and MCMC strategy [34] which is briefly reviewed in Appendix A. TMCMC provides ultimately N_s samples from each intermediate density and, ultimately, from posterior $p(\theta_t|\mathbf{D})$ as well as an estimate for the normalization constant for the latter (denominator of Eq. (8)). This normalization constant represents the so-called evidence for the data [22], and though it does not play a critical role in

the definition of the posterior PDF $p(\theta_t|\mathbf{D})$, it is relevant for the model class selection task that will be discussed in the next section. In particular, the evidence of the system could be estimated by the following expression [34,35]:

$$P(\hat{\mathbf{h}}\Big|\hat{\mathbf{W}}) = \prod_{j=1}^{n}\left[\frac{1}{N_s}\sum_{p=1}^{N_s} p\left(\hat{\mathbf{h}}\Big|\,\theta_{t(j)}^{p},\hat{\mathbf{W}}\right)^{q_j-q_{j-1}}\right] \tag{12}$$

where $\theta_{t(j)}^{p}$ corresponds to the p-th sample generated in j-th TMCMC level from intermediate density $p_j(\theta_t|\mathbf{D})$. The quantity in the brackets in Eq. (12) represents the weight mean $\hat{S}_{j+1}$ discussed in Appendix A.

2.4. Model class selection

Beyond the parameter updating, the Bayesian inference scheme also supports the selection of the best/optimal model in a specified class of models. To formalize this idea, let $U = \bigcup_{i=1}^{N} U_i$ denote a set containing different classes of models with U_i representing the ith model. Each of these models provides a different output function $H_i(\theta_i,\omega)$ and includes n_i-dimensional parameter vector $\boldsymbol{\theta}_i$. Conditional on the experimental data $\mathbf{D}$ the posterior for each model class, representing the updated probability (based on measurements) of the i-model over the whole set of models, is obtained using the Bayes' theorem as:

$$P(U_i|\mathbf{D},U) = \frac{P(\mathbf{D}|U_i)P(U_i)}{\sum_{i=1}^{N} P(\mathbf{D}|U_i)P(U_i)} = \frac{P(\hat{\mathbf{h}}\Big|\hat{\mathbf{W}},U_i)P(U_i)}{\sum_{i=1}^{N} P(\hat{\mathbf{h}}\Big|\hat{\mathbf{W}},U_i)P(U_i)} \tag{13}$$

where $P(U_i)$ is the prior for the model class (indicating the prior believe of the adequacy of the i-model compared to the whole set of models) and $P(\mathbf{D}|U_i) = P(\hat{\mathbf{h}}\Big|\hat{\mathbf{W}},U_i)$ is the evidence for the model class, corresponding to the denominator of Eq. (8), and representing, ultimately, the marginal likelihood of the i-model given the data. The posterior probability $P(U_i|\mathbf{D},U)$ represents a rational approach for selecting the most appropriate model as inferred from the data, or for choosing the weights for the predictions that come from each model if all of them are going to be used for that purpose (model class averaging) [21]. Note that this approach automatically enforces the principle of model parsimony: the model chosen using $P(U_i|\mathbf{D},U)$ balances between model accuracy and model complexity. In other words, more complex models that provide better fit to the data are not necessarily chosen as the better ones since ranking using $P(U_i|\mathbf{D},U)$ automatically accounts also for model complexity [21].

For estimating $P(U_i|\mathbf{D},U)$ using Eq. (13) the challenging aspect is the estimation of the evidence. For systems that are globally identifiable this can be done using Laplace's asymptotic expansion [23,22], leading to:

$$P(\hat{\mathbf{h}}\Big|\hat{\mathbf{W}},U_i) = \frac{(2\pi)^{n_i/2} p\left(\hat{\mathbf{h}}\Big|\,\theta_{t(i)}^{MAP},\hat{\mathbf{W}}\right) p\left(\theta_{t(i)}^{MAP}\right)}{\sqrt{\det\left[-\mathbf{H}_s(\theta_{t(i)}^{MAP})\right]}} \tag{14}$$

where n_i is the number of model parameters employed in the i-model, $p\left(\hat{\mathbf{h}}\Big|\,\theta_{t(i)}^{MAP},\hat{\mathbf{W}}\right)$ is the likelihood function using the ith-model $H_i(\theta_i,\omega)$, $p\left(\theta_{t(i)}^{MAP}\right)$ corresponds to the prior PDF for the model parameters of the model, while $\mathbf{H}_s(\theta_{t(i)}^{MAP})$ corresponds to the Hessian matrix of Eq. (11) for the model, with all three latter quantities evaluated at the MAP value of the ith-model. Accuracy of Eq. (14) is dependent, as discussed in previous section, on how peaked the posterior distribution is. For cases in which Laplace's method of asymptotic approximation is inadequate, meaning typically not globally identifiable systems or applications with small set of experimental data (asymptotic characteristics are not guaranteed), the evidence should be computed via Monte Carlo simulations, for example in the TMCMC setting through Eq. (12) [22] as discussed in the previous section.

3. Model parameter updating for PEHs

The Bayesian inference/updating scheme requires following information: (1) experimental data for the PEH output (2) a system model to predict that output and (3) a prior PDF to define the relative likelihood of the system model parameters (or even the different model classes when model class selection is performed). Here as output the FRF of PEHs is chosen and the setting described in [11,12] is adopted to provide the required information to perform Bayesian updating.

3.1. System model for FRFs in PEHs

The adopted system model for obtaining the FRF of PEHs corresponds to the widely used Analytical Distributed Parameter Solution (ADPS) proposed by Erturk and Inman [3], relying on a standard modal expansion assuming an Euler-Bernoulli

beam model. According to this model the FRF of PEHs, with input the PEH acceleration and output the voltage generated, is expressed as function of the electro mechanical and geometrical characteristics of the harvester as:

$$H(\theta,\omega)=\left(\frac{i\omega}{i\omega+k_{pzt}}\boldsymbol{\varphi}^T\right)\left[-\mathbf{I}\omega^2+i\omega\mathbf{C}_{eq}+\mathbf{K}_{eq}+\frac{1}{i\omega+k_{pzt}}\boldsymbol{\chi}\boldsymbol{\varphi}^T\right]^{-1}\mathbf{r} \tag{15}$$

where $\mathbf{I}$, $\mathbf{C}_{eq}$, and $\mathbf{K}_{eq}$ are M_o-by-M_o matrices corresponding to equivalent mass, damping and stiffness, respectively, with M_o being the number of eigenvectors used in the modal expansion and χ, φ, and $\mathbf{r}$ are M_o-by-1 vectors representing, respectively, electrical coupling, mechanical coupling and mechanical forcing amplification. The term k_{pzt} is a scalar value representing the combined electrical characteristics of the harvester (represents combined effect of the electric resistance and the piezoelectric layer capacitance). All aforementioned quantities, including matrices $\mathbf{I}$, $\mathbf{C}_{eq}$, and $\mathbf{K}_{eq}$, vectors χ, φ, and $\mathbf{r}$ and scalar k_{pzt} are directly related to the geometry of the harvester and its electro-mechanical properties. These relations are not presented here, however, they are fully described in a previous work of the authors (please refer to appendix of [12]). The model parameter vector θ is defined as the vector containing all necessary parameters (geometric characteristics and electro-mechanical properties) needed in these relationships:

$$\theta=\begin{bmatrix}\zeta & s_{11}^E & d_{31} & \varepsilon_{33}^T/\varepsilon_o & \rho_p & \rho_s & Y_s & L & b & h_s & h_p\end{bmatrix} \tag{16}$$

The above variables correspond to the length L, the width b, the thickness of the piezoelectric layer h_p, the thickness of the substructure h_s, the substructures density ρ_s, the piezoelectric layers density ρ_p, the Young Modulus of the substructure Y_s, the elastic compliance at constant electric field s_{11}^E, the piezoelectric strain constant d_{31}, the permittivity at constant stress ε_{33}^T, the permittivity constant ε_o, and the damping ratio ζ.

3.2. Prior probability density function for model parameters

Recently, Ruiz and Meruane [11] reported typical variations associated with the geometric characteristics of PEHs as well as variations reported by manufacturers for the electro-mechanical properties of the materials used in these devices. In general, variability can extend to 25–30% of the nominal characteristic, especially for electro-mechanical properties. As mentioned in the introduction, PEHs are composed of layers of piezoelectric materials bonded to a layer that serves as structural support. With respect to the description of the device properties, the biggest challenge is related to the characterization of the sub-structural layer (please refer to Fig. 1) since the mathematical models usually consider a single substructural layer neglecting the effect of the bond material [44]. Moreover, some manufacturers employ composite materials in the substructure without fully reporting their mechanical characteristics [11]. As a consequence, the uncertainty associated with the mechanical properties of the substructure layer is large. On the other hand, variability associated with the geometrical characteristics of the harvesters is small, frequently not exceeding 3% of nominal values [12]. These observations can guide the selection of the prior probability model, which will still be application dependent since it is a function of the available information for the examined device, i.e. confidence related to its geometrical and electromechanical properties. In this study, for $p(\theta)$ independent lognormal distribution are adopted for each property with a median equal to the nominal parameter values and coefficient of variation reflecting the anticipated variability based on the available information. Should be pointed out that selection of lognormal distributions can be justified through the use of maximum information entropy principle [45] as the distribution incorporating the largest amount of uncertainty in the model description given the available information and the additional constraint that the modeled properties take positive values.

3.3. Experimental identification of the FRF

For obtaining the measurement data for the FRF of PEHs the experimental procedure recently proposed by Peralta et al. [12] is adopted. The procedure allows the definition of the FRF at a number of frequencies using a sweep sine excitation. Leveraging high precision instruments, each test provides a practically noise-free smooth experimental FRF giving for M desired frequencies $\{\hat{\omega}_m; m=1,...,M\}$ (input) the FRF values $\left\{\hat{h}_m; m=1,...,M\right\}$ (output) representing the input/output observation data. When repeating this experimental procedure multiple times slight variation of the observations is reported, particularly with respect to the frequency corresponding to the FRF peak (fundamental frequency of the PEH). This should be attributed to uncontrollable variables impacting the experiments, presumably dealing with the clamping mechanisms of the PEH (boundary condition) and friction between elements. There are multiple approaches to accommodate these variations within the model updating setting, for example identifying the posterior distribution of the model parameters to match the entire distribution of the observations (both mean and variability) [46,47]. Since the variability observed in the commercial PEHs response in the illustrative case study is quite low (see discussion in Section 4) a different path is adopted here: the results from multiple experiments are averaged to remove the influence of the aforementioned uncontrollable variables in the experimental set-up. This approach maintains also the intended emphasis of the paper on the fundamentals of the Bayesian model updating implementation, so that results and relevant discussions are not impacted by the influence of uncontrollable settings in the experimental set up, which is the source of the measured variability in the obser-

vations here. An extension to use all the measurements, instead of the mean observations, will be also briefly discussed to demonstrate the influence of the observation variability on the identified model parameters.

3.4. Prior and posterior predictive analyses

Predictive analysis for PEHs refers to the estimation of the frequency response for specific frequencies, incorporating all available information for the PEH model characteristics. Depending on the source for the latter one, can distinguish between nominal, prior or posterior predictions, using respectively, the nominal parameter values (deterministic predictions), the prior probabilistic description $p(\theta_t)$ and the posterior probabilistic description $p(\theta_t|\mathbf{D})$. When the latter two are utilized, the propagation of the model parameter uncertainties to the predicted output is needed, using typically the total probability theorem. In this setting, the prior expected FRF value for a given excitation frequency ω, which is the main quantity of interest, is:

$$E[h|\omega] = \int E[h|\theta_t, \omega]p(\theta_t)\ d\theta_t = \int H(\theta, \omega)p(\theta)\ d\theta \tag{17}$$

where expectation $E[h|\theta_t, \omega]$ is with respect to the prediction error and the second equality in Eq. (17) uses the fact that under the common assumptions for this error (unbiased predictions) $E[h|\theta_t, \omega] = H(\theta, \omega)$. The multidimensional integral in Eq. (17) can be solved using Monte Carlo Integration. For the posterior expected FRF value, the prior distribution in Eq. (17) needs to be replaced with the posterior, leading to

$$E[h|\omega, \mathbf{D}] = \int E[h|\theta_t, \omega]p(\theta_t|\mathbf{D})\ d\theta_t = \int H(\theta, \omega)p(\theta|\mathbf{D})\ d\theta \tag{18}$$

This integral can be similarly calculated through Monte Carlo integration, utilizing TMCMC to obtain samples from $p(\theta|\mathbf{D})$. An alternative approach is to use Laplace's asymptotic approximation which leads to $E[h|\omega, \mathbf{D}] = H(\theta^{MAP}, \omega)$ [48].

4. Case study for commercial bimorph PEHs

The Bayesian inference methodology discussed in the previous section is applied to bimorph PEHs. The PEHs used here correspond to two devices with different lengths, similar to the one used previously in [12]. Devices will be referenced herein as PEH-A (Model A) and PEH-B (Model B) with the first (Model A) corresponding to the longer device. The nominal characteristics of the devices are presented in the first columns of Table 1. As mentioned in Section 3.3. the FRF of the PEHs was identified multiple times following the procedure presented in [12]. Variability of observations for PEH-A was very low, with coefficient of variation in the range of 1–2%, and bit higher for PEH-B, with coefficient of variation in range of 2–4%. As discussed in Section 3.3 to account for this small variability, stemming from uncontrollable parameters in the experimental set-up, the mean of the experimental data is mainly considered here as the experimental observations. An extension to consider all the data will be also discussed at the end of this section. Fig. 2 presents the experimental FRF for the PEHs along with their nominal predictions (corresponding to nominal parameter). The figure verifies the potential significant differences between the nominal prediction and the experimental FRF, a result in agreement with [12].

For the prior probability model $p(\theta)$ independent lognormal distributions are assumed with median corresponding to the nominal values and coefficient of variation equal to 5% for the geometrical characteristics and 30% for the electromechanical properties (also reported in Table 1). Choice for coefficient of variation reflects the observation that geometric characteristics

Table 1
Nominal characteristics of the PEHs tested together with the prior model. The prior model corresponds to a lognormal distribution with the given median and coefficient of variation (latter reported in parenthesis).

Model parameters	Nominal		Prior	
	PEH-A	PEH-B	PEH-A	PEH-B
ρ_s[kg m^{-3}]	N/R*	N/R*	7400 (100%)	7400 (100%)
E_s[GN m^2]	N/R*	N/R*	61 (100%)	61 (100%)
s_{11}^E[pN^{-1} m^2]	16.4	16.4	16.4 (30%)	16.4 (30%)
$-d_{31}$ [pC N^{-1}]	320	320	320 (30%)	320 (30%)
$\varepsilon_{33}^T/\varepsilon_o$[F m^{-1}]	4500	4500	4500 (30%)	4500 (30%)
ρ_p[kg m^{-3}]	7400	7400	7400 (30%)	7400 (30%)
L [mm]	40.0	23.5	40.0 (5%)	23.5 (5%)
b [mm]	10.05	10.05	10.05 (5%)	10.05 (5%)
h_p[mm]	0.248	0.248	0.248 (5%)	0.248 (5%)
h_s[mm]	0.234	0.234	0.234 (5%)	0.234 (5%)
ζ	N/R*	N/R*	0.017 (30%)	0.017 (30%)

$\varepsilon_o = 8.854 \times 10^{-12}$.
N/R indicates "not-reported" by the manufacturer.
*To perform nominal predictions it is assumed as the median of the prior PDF.

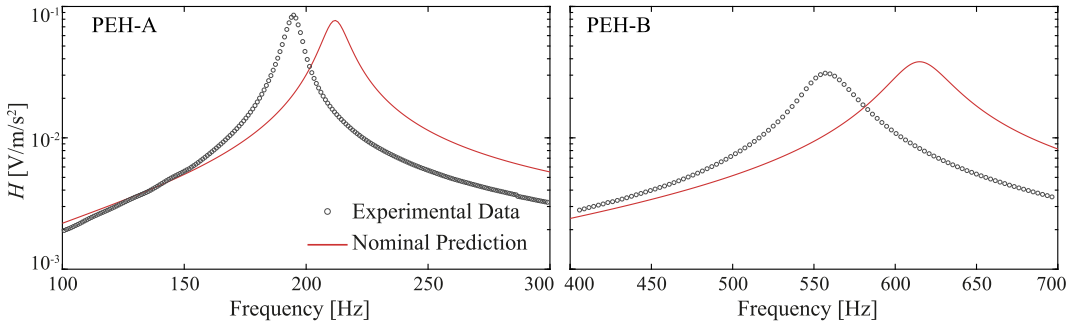

Fig. 2. Comparison of the nominal prediction (model corresponding to nominal model parameters) and the experimental FRF (for 100 frequency points) for both PEH models studied.

can be measured with a high degree of certainty whereas electromechanical properties reported by manufacturers [49] show typical variability in 20–30% range. With respect to the properties of the substructure layer no detailed nominal information was directly available by the manufacturer beyond the fact that it was made by a composite of carbon fiber, silver and an adhesive material. For this reason, it is decided to assumed that the piezoelectric and the substructure layers have the same Young's modulus and density but introducing a higher degree of variation (coefficient of variation equal to 100%) to account for the limited information.

The Bayesian inference scheme is applied to the two PEH devices to update the model parameters, including their variability and perform predictive analysis. In addition, model class selection is discussed, with the different classes obtained by considering only subsets of the model parameters as uncertain (more details on this later). A range of different settings of the Bayesian framework are examined with respect to the impact of the prediction error model or the computational tools used to perform the Bayesian inference. Unless otherwise stated, all parameters reported in Table 1 are updated, while the observation data correspond to FRF values in frequency range 100–300 Hz and 400–700 Hz for PEH A and B, respectively, with discretization taken to correspond to a total of $M = 100$ observation data for each case. With respect to the application of point estimates using Laplace's asymptotic expansion, the prior distributions reported in Table 1 are transformed to the standard Gaussian space. Discussion starts with examining the influence of the prediction error.

4.1. Impact of prediction error model

An important component of the Bayesian inference framework is the exact model assumed for the prediction error and, subsequently, for the likelihood function [Eqs. (6) and (7), for additive and multiplicative prediction error, respectively]. Independent of the exact selection, recall that the error dispersion, quantified through σ_e is incorporated in the augmented model parameter vector θ_t and updated with the rest of model parameters θ. The prior for σ_e is taken to be a lognormal distribution with median 0.15 V/m/s^2 and coefficient of variation of 400% for the additive error and with median 1.5 and coefficient of variation 400% for the multiplicative error. The large coefficient of variation values reflect the limited prior information about this error.

The impact of the error is examined first with respect to the point MAP estimate for θ_t, identified by solving Eq. (9) using the respective likelihood function for each error case. Results are presented in Table 2 for each of the error cases as well as for the relative absolute difference between these cases. It is evident that the assumption for the error has small influence for all parameters except for the ε_{33}^T for which large discrepancies exist. Further insight for the impact of the error assumption is examined by looking at the expected median posterior predictions $H\left(\theta^{MAP},\omega\right)$ as well as the predictions within 3 standard deviations from the median when considering the prediction error variability. For the additive error model the latter is given by $H\left(\theta^{MAP},\omega\right)\pm 3\sigma_e^{MAP}$ and for the multiplicative error by $H\left(\theta^{MAP},\omega\right)\ln(3\sigma_e^{MAP})\approx H\left(\theta^{MAP},\omega\right)(1\pm 3\sigma_e^{MAP})$. Results are presented in Fig. 3. First row presents the comparison between the experimental FRF (grey circles), and the (median) model output employing the MAP values for the additive (blue) or the multiplicative prediction error (red). FRF predictions established by using either error are very similar and match very well the experimental data, with the predictions corresponding to the multiplicative error (red line) providing a slightly better match. Second row of Fig. 3 presents the confidence intervals within three standard deviations of the median predictions. These results demonstrate that a drawback of the additive error assumption of Eq. (1) is that is does not scale with the output amplitude, leading to large variability for the lower FRF amplitudes, a drawback that does not exist for the multiplicative error, creating variability that is proportional to the amplitude. In other words, the coefficient of variation of the FRF increases far from the FRF peak or it remains constant along the frequencies depending if the prediction error is additive or multiplicative, respectively.

Overall these discussions demonstrate that the prediction error assumption has little influence on the parameter values obtained through Bayesian model updating. The larger differences identified for ε_{33}^T should be attributed to small sensitivity

Table 2
MAP values of the posterior PDF employing additive and multiplicative prediction errors. The relative absolute difference between the identified values) are reported as percentage in parenthesis.

Model Parameters	PEH-A		PEH-B	
	Additive	Multiplicative	Additive	Multiplicative
ρ_s[kg m^{-3}]	7023	72643 (3%)	7413	7503 (1%)
E_s[GN m^2]	63.3	62.7 (1%)	58.6	58.5 (<0.5%)
s_{11}^E[pN^{-1} m^2]	17.7	18.25 (3%)	17.3	16.8 (3%)
$-d_{31}$ [pC N^{-1}]	262.4	261.4 (<0.5%)	317.7	325.7 (2%)
$\varepsilon_{33}^T/\varepsilon_o$[F m^{-1}]	12,066	8466 (43%)	9994	11,903 (17%)
ρ_p[kg m^{-3}]	7321	7372 (1%)	7402	7428 (<0.5%)
L [mm]	40.9	40.6 (1%)	24.1	24.2 (<0.5%)
b [mm]	10.3	10.1 (1%)	10.2	10.3 (<0.5%)
h_p[mm]	0.242	0.244 (1%)	0.242	0.241 (<0.5%)
h_s[mm]	0.234	0.234 (<0.5%)	0.234	0.234 (<0.5%)
ζ	0.013	0.013 (4%)	0.021	0.021 (<0.5%)
σ_e [V/m/s^2]	5.74 × 10^{-4} 0.0219	1.27 × 10^{-4} [V/m/s^2]	0.0101	
$\ln\left(p\left(\hat{\mathbf{h}}\middle\vert \theta_t^{MAP}, \hat{\mathbf{W}}\right)\right)$	610.5164	242.7247	763.3272	320.5653

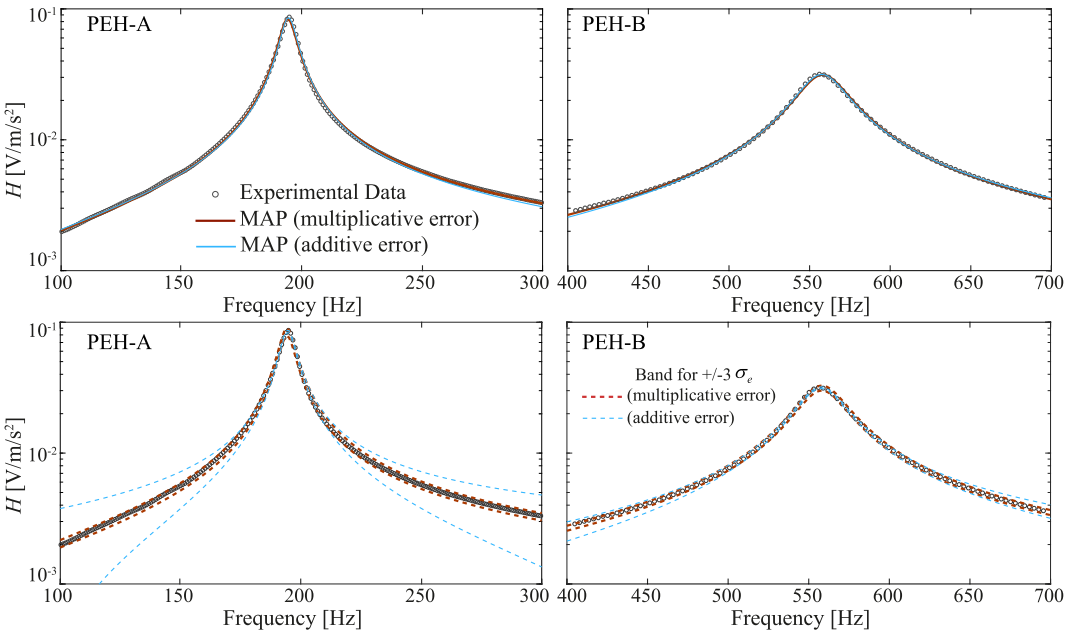

Fig. 3. Estimation of the FRF for MAP values adopting either an additive or multiplicative prediction error for PEH-A (left column) and PEH-B (right column). Top row shows FRF without prediction error while bottom row shows in dotted lines the confidence interval corresponding to ±3 standard deviations for the prediction error. Experimental FRFs are also shown.

of the FRF response to that parameter, as also showcased by the fact that the FRF predictions in Fig. 3 are very similar, despite these differences. On the other hand, the error assumption impacts the variability of the predictions, with additive error creating disproportionally large variability for lower FRF amplitude values, indicating that a multiplicative error is more reasonable for the PEH FRF-based identification setting. This is the assumption for the prediction error utilized in the remainder of the study.

4.2. Difference between point estimates (MLE and MAP) and complete posterior distribution approximation

The discussion moves next to the different approaches for characterizing the posterior distribution, using either a point estimate (MAP or MLE) or using the entire distribution with samples obtained through TMCMC.

For the MLE optimization of Eq. (10), which recall is equivalent to the MAP one in Eq. (9) when considering a flat (uniform) prior, multiple local minima are identified, showing that problem is not globally identifiable. Actually these local minima, identified here through gradient-based solver for Eq. (10) with different starting points for each trial, correspond to

practically same value for the likelihood function, meaning they are all equally plausible. This characteristic provides a strong indication that there might be a manifold of MLE parameters with same preference (unidentifiable problem). In contrast, for the MAP optimization of Eq. (9) a single global optimum is identified. This difference between MLE and MAP is actually common for many Bayesian inference problems; the sensitivity introduced through the prior distribution function allows to differentiate them in the MAP context even though they correspond to the same likelihood function value (all are MLE parameters). Still the low sensitivity of the posterior PDF values across these points, introduced only through the prior and not, additionally, through the likelihood function, means that accuracy of point estimation methods is somewhat reduced. This can be verified by looking at the minimum eigenvalue λ of $\mathbf{H}_s(\theta_t^{MAP})$; in such instances it is expected that $1/\sqrt{\lambda}$ will be large compared to the same value for the prior distribution. In particular, maximum value of $1/\sqrt{\lambda}$ is estimated to be equal to 1.0288 and 1.0775 for PEH-A and PEH-B, respectively, meaning that the max curvature of the posterior is practically identical to the curvature of the prior (note that problem was formulated in standard Gaussian space). This means that asymptotic characteristics of Laplace's expansion no longer hold (posterior is not peaked) and that any approximation using that expansion will be accurate only if the posterior ends up being actually a Gaussian distribution.

Table 3 presents two indicative MLE optima for the model parameters, denoted as $\theta_t^{MLE_1}$ and $\theta_t^{MLE_2}$, along with the relative difference between them, shown in parenthesis. The model characteristic that presents the most important variation between the two MLE optima, indicating that there is a low sensitivity for the predicted FRF with respect to its value, is the elastic modulus of the substructure layer (E_s). For the MAP optimization the global maximum has been already presented in Table 2 earlier. The absolute relative difference between MAP and MLE values is presented in Table 4, highlighting that the introduction of the prior PDF can have a considerable impact on the model parameter estimation, at least for some of them, with estimates for the electromechanical properties of the PEH differing by as much as 10%. The more interesting comparison is, though, with respect to the predicted FRFs shown in Fig. 4 for both the MAP and MLE model parameters. It is evident that all approaches offer similar FRF estimation, and in all instances in very good agreement with the experimental data, verifying our claim earlier that difference in the identified model parameters represents a trade-off in the way they impact FRF

Table 3
Two different updated model parameters employing MLE. The relative difference between them is shown in parenthesis.

Model Parameters	PEH-A		PEH-B	
	$\theta_t^{MLE_1}$	$\theta_t^{MLE_2}$	$\theta_t^{MLE_1}$	$\theta_t^{MLE_2}$
ρ_s[kg m^{-3}]	8138	8112 (<0.5%)	8186	8140 (1%)
E_s[GN m^2]	63.0	58.6 (7%)	60.4	57.9 (4%)
s_{11}^E[pN^{-1} m^2]	18.6	18.6 (<0.5%)	17.9	17.9 (<0.5%)
$-d_{31}$ [pC N^{-1}]	267.5	267.5 (<0.5%)	349.1	349.6 (<0.5%)
$\varepsilon_{33}^T/\varepsilon_o$[F m^{-1}]	8975	8987 (<0.5%)	12,744	12,766 (<0.5%)
ρ_p[kg m^{-3}]	7467	7466 (<0.5%)	7484	7479 (<0.5%)
L [mm]	40.1	40.1 (<0.5%)	23.8	23.8 (<0.5%)
b [mm]	9.9	9.9 (<0.5%)	10.0	10.0 (<0.5%)
h_p[mm]	0.247	0.248 (<0.5%)	0.245	0.245 (<0.5%)
h_s[mm]	0.233	0.233 (<0.5%)	0.233	0.233 (<0.5%)
ζ	0.013	0.013 (<0.5%)	0.021	0.021 (<0.5%)
σ_e	0.0219	0.0219	0.0101	0.0101
$\ln\left(p\left(\hat{\mathbf{h}}\middle\vert \theta_t^{MLE}, \hat{\mathbf{W}}\right)\right)$	242.7748	242.7748	320.5829	320.5829

Table 4
Relative absolute difference between MAP and MLE model parameters.

Model Parameters	PEH-A		PEH-B	
	$\left\vert\frac{\theta_t^{MAP}-\theta_t^{MLE_1}}{\theta_t^{MAP}}\right\vert x100$	$\left\vert\frac{\theta_t^{MAP}-\theta_t^{MLE_2}}{\theta_t^{MAP}}\right\vert x100$	$\left\vert\frac{\theta_t^{MAP}-\theta_t^{MLE_1}}{\theta_t^{MAP}}\right\vert x100$	$\left\vert\frac{\theta_t^{MAP}-\theta_t^{MLE_2}}{\theta_t^{MAP}}\right\vert x100$
ρ_s[kg m^{-3}]	12%	12%	9%	8%
E_s[GN m^2]	<0.5%	7%	3%	1%
s_{11}^E[pN^{-1} m^2]	2%	2%	7%	7%
$-d_{31}$ [pC N^{-1}]	2%	2%	7%	7%
$\varepsilon_{33}^T/\varepsilon_o$[F m^{-1}]	6%	6%	7%	7%
ρ_p[kg m^{-3}]	1%	1%	1%	1%
L [mm]	1%	1%	2%	2%
b [mm]	2%	2%	3%	3%
h_p[mm]	1%	1%	2%	2%
h_s[mm]	<0.5%	<0.5%	<0.5%	<0.5%
ζ	1%	<0.5%	<0.5%	<0.5%
σ_e	<0.5%	<0.5%	<0.5%	<0.5%

predictions (i.e., provide same FRF values) and not a trade-off in the way they fit the different observations. Both the MLE and the MAP point estimates facilitate a very good match with respect to the predicted FRF, though if the interest is in identifying the actual model parameters themselves, then the MAP facilitates a global identification. The differentiation offered by the MAP approach though, is primarily influenced by the prior information, indicating the importance of the engineering judgment guiding that selection.

For obtaining more comprehensive information about the electromechanical properties of the PEHs in a Bayesian setting the entire posterior PDF is further identified using the TMCMC algorithm. Results are presented in Figs. 5 and 6 for PEH-A and PEH-B, respectively, showing histograms for each component of θ_t (in other words samples from the marginal posterior distributions) and comparing each of them to their respective nominal (red solid line) and MAP values (blue dashed line). The coefficient of variation (c.o.v) obtained through the samples is also reported in each of the figures. The results show that, as expected, the MAP values provide a good approximation of the peak of the posterior PDF, as in all cases they are close to the peaks of the marginal distributions, expected to be in close proximity to the peak of the joint posterior distribution. On the other hand significant differences are evident between MAP and nominal values, with larger differences reported for the modal damping ζ, the elastic compliance at constant electric field s_{11}^E, the piezoelectric strain constant d_{31}, and the permittivity at constant stress ε_{33}^T. With respect to the variability of the posterior distribution, large spread is noted for many model

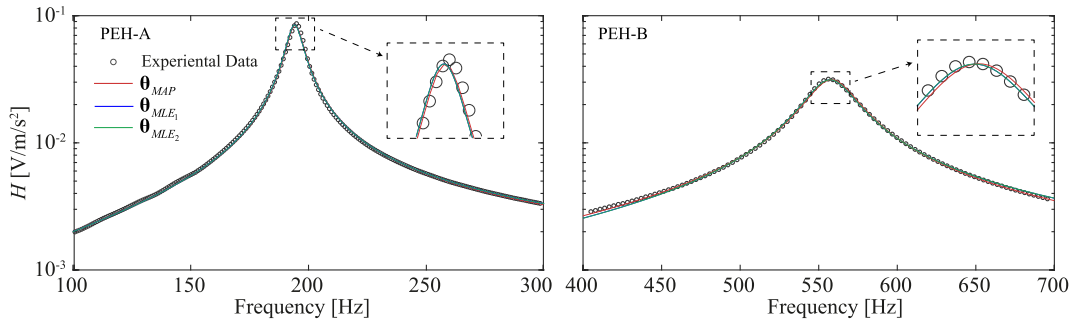

Fig. 4. Expected FRF utilizing either MAP or MLE (results corresponding to two maxima MLE points) values for the model parameters for the implementation considering multiplicative prediction error. Experimental results are also presented. A zoom close to the maximum of the FRF is included to highlight small discrepancies between experimental data and predictions for the different MAP/MLE parameters.

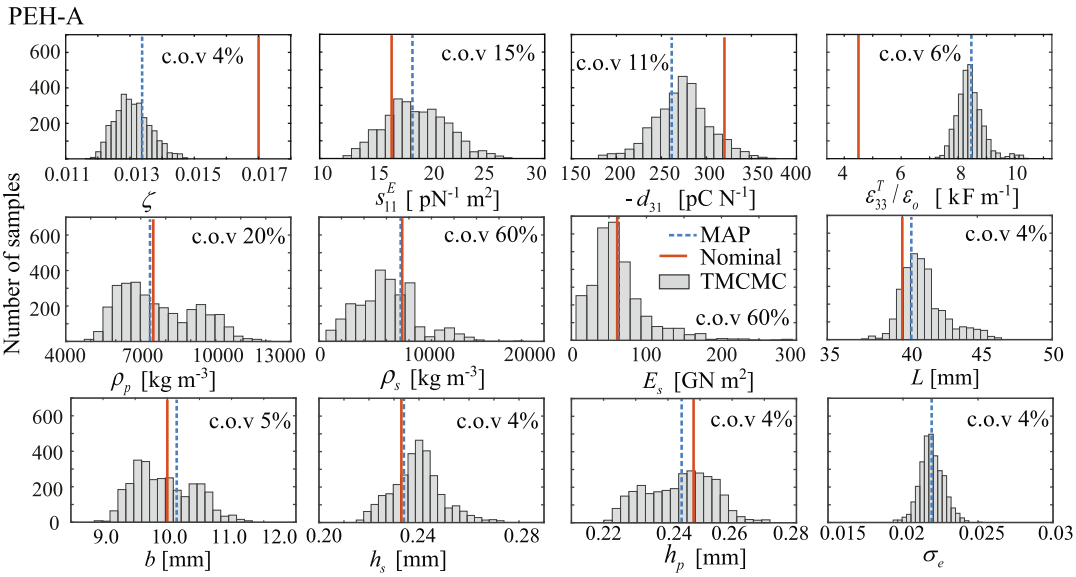

Fig. 5. Histograms of samples from posterior obtained with TMCMC for PEH-A. MAP and nominal values are also presented in dashed blue and solid red lines, respectively. Coefficient of variation for each marginal model parameter is also shown. (For interpretation of the references to color in this figure legend, the reader is referred to the web version of this article.)

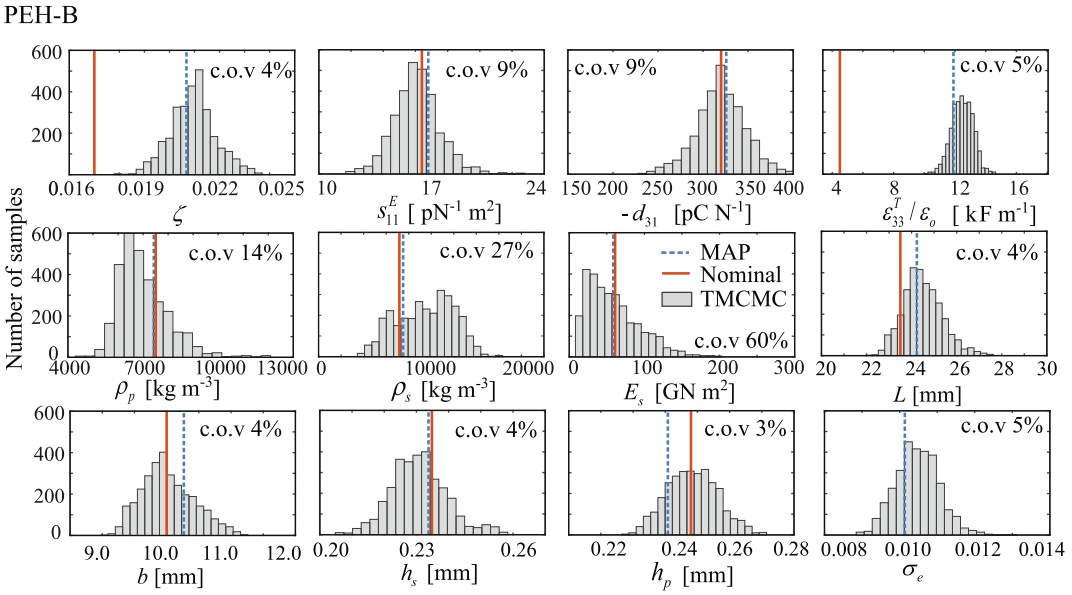

Fig. 6. Histograms of samples from posterior obtained with TMCMC for PEH-B. MAP and nominal values are also presented in dashed blue and solid red lines, respectively. Coefficient of variation for each marginal model parameter is also shown. (For interpretation of the references to color in this figure legend, the reader is referred to the web version of this article.)

parameters, with c.o.v reaching 60% for the parameters associated with the substructure (E_s and ρ_s) and 20% for the electromechanical properties of the piezoelectric layer, while remaining below 5% for the geometrical characteristics. For some PEH model characteristics this represents a moderate only reduction compared to the prior distribution, indicating once again the relatively significant trade-off in the way these characteristics impact FRF predictions.

The histograms in Figs. 5 and 6 demonstrate also that the posterior PDF is not well approximated by a Gaussian. This is better illustrated in Figs. 7 and 8 that show the marginal posterior distributions for each model parameter obtained either through the fitted Gaussian approximation or through Kernel density estimation using the TMCMC samples from Figs. 5 and 6, respectively. Note that plots are expressed with respect to the model parameter space to maintain consistency with the presentation is Figs. 5 and 6, and not in the standard Gaussian space with respect to which the fit is initially established. This is why the Gaussian fit in Figs. 7 and 8 is no longer a Gaussian, but rather a lognormal distribution. It is evident that there is a poor match between the two PDFs, with samples from the posterior $p(\theta_t|\mathbf{D})$ exhibiting in some instances even bi-modal characteristics, indicating that unfortunately the Gaussian fit is not a valid assumption for the posterior distribution. Furthermore, since posterior has been already identified to violate the asymptotic features of Laplace's expansion, point-estimates are expected to offer a poor approximation for estimating higher order statistics (beyond the MAP values) for the PEH application.

The trade-off between the model characteristics is further investigated by looking at the correlation between them, something not depicted when focusing only on the marginal distributions in Figs. 5 and 6. The correlation coefficient of the TMCMC samples for the posterior distribution is reported in Fig. 9 for the PEH-A model. Trends for PEH-B are similar and are not being reported due to space limitations. To help visually distinguish between the different correlation levels, red color bars are used for parameters with correlation exceeding 0.7 (significant correlation), yellow color bars for variables with correlation above 0.4 but below 0.7 (moderate correlation) and green for the rest. Significant correlation exists between ζ, s_{11}^E, ρ_p and d_{31}, while on the other hand model parameters E_s, h_s, and σ_e are practically uncorrelated from the rest. These trends verify the potential trade-off between model characteristics in the way they impact the FRF predictions; since the prior distributions for the model parameters are independent, the correlation in the posterior stems from the likelihood function, and ultimately from the FRF model predictions.

To further investigate the effect of the parameter correlation the 90% confidence interval for the FRF prediction is shown in Fig. 10. The probability that H will exceed threshold H_t is considered, given by,

$$P(H \geqslant H_t) = \int I_F(\theta_t, \omega) p(\theta_t|\mathbf{D}) d\theta_t \tag{19}$$

where the indication function $I_F(\theta_t, \omega)$ is equal to zero if $H(\theta, \omega)e < H_t$ and to one if $H(\theta, \omega)e \geqslant H_t$. The thresholds corresponding to $P(H > H_t^u) = 0.95$ and $P\left(H > H_t^l\right) = 0.05$ are then identified and define the 90% confidence interval around the median FRF predictions for each frequency. Estimation of the probabilities through Eq. (19) is performed through Monte Carlo simulation using samples from $p(\theta_t|\mathbf{D})$, readily available through the TMCMC implementation. In addition to using the

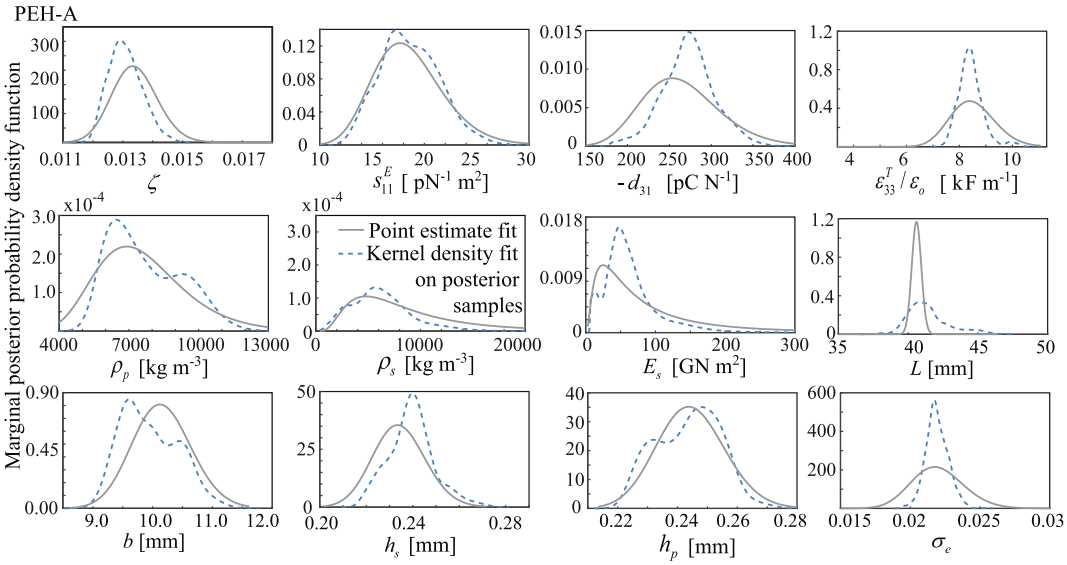

Fig. 7. Posterior PDF for PEH-A approximated either through a point estimate (Gaussian) fit or through Kernel density estimation using samples for posterior obtained through TMCMC.

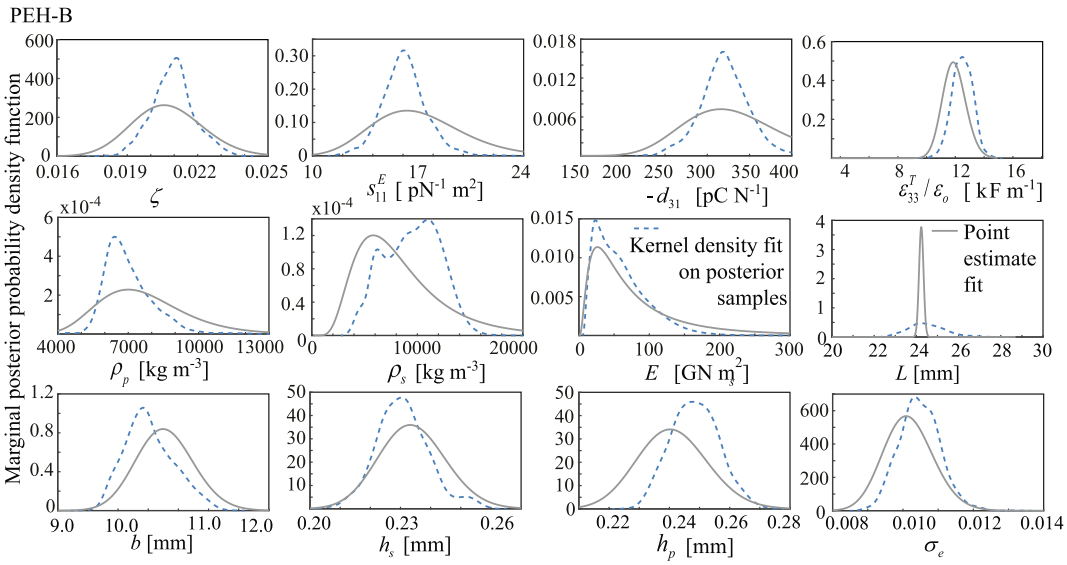

Fig. 8. Posterior PDF for PEH-B approximated either through a point estimate (Gaussian) fit or through Kernel density estimation using samples for posterior obtained through TMCMC.

actual posterior distribution (red domain in Fig. 10) two other cases are examined; (a) fit independent distributions on the marginals resulting from $p(\theta_t|\mathbf{D})$ [Figs. 5 and 6] and use these distributions in place of actual $p(\theta_t|\mathbf{D})$ (light green domain in Fig. 10) or (b) use the Gaussian fitted distribution discussed in Section 3.2 with mean the MAP value, and covariance matrix the inverse of the Hessian in Eq. (11) (dark green domain in Fig. 10). First approximation ignores the correlation in the identified posterior distribution whereas second approximation relies on a Gaussian fit over the peak of the posterior distribution. Results show that the use of the actual $p(\theta_t|\mathbf{D})$ provides a very narrow confidence interval for the FRF predictions, something that does not hold for the case that uncorrelated distributions are assumed. This provides a very strong verification of our previous claims; although the identified model parameters are associated with large coefficients of variation (Figs. 5 and 6), the correlation between these parameters (presented in Fig. 9) and the trade-offs these represent, result in a very small dispersion in the FRF predictions. Ignoring the parameter correlations leads to significant deviation from this

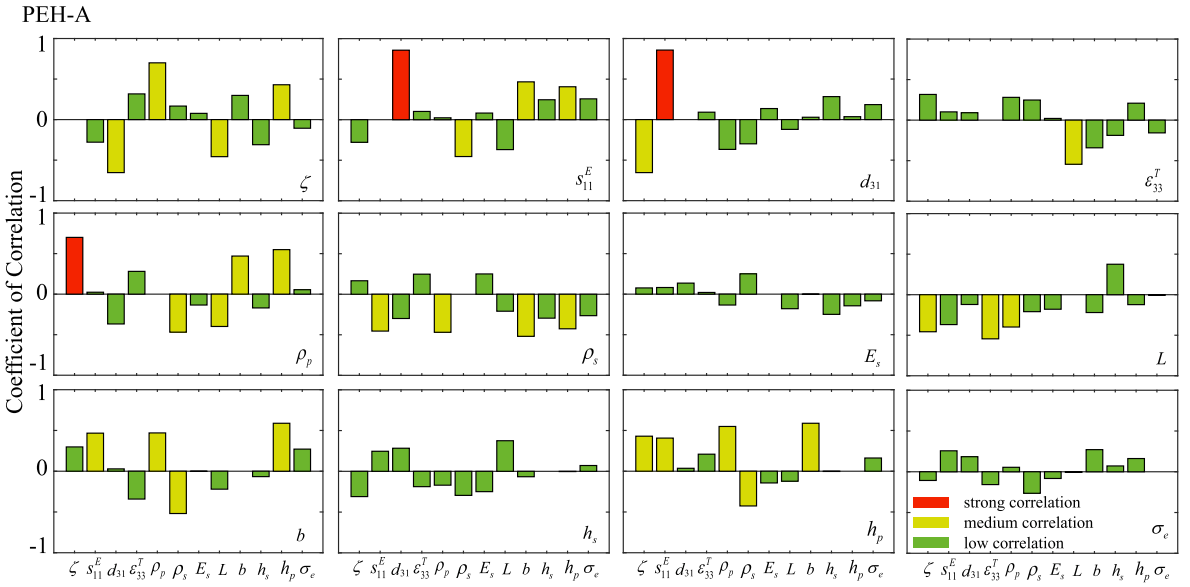

Fig. 9. Correlations coefficients for PEH-A parameters (obtained using TMCMC).

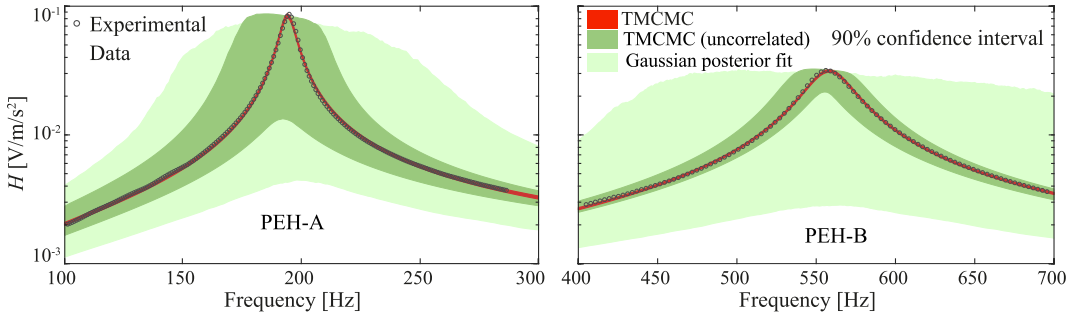

Fig. 10. FRF with confidence interval of 90% is presented for both PEHs studied obtained by: a) TMCMC samples directly from $p(\theta_t|\mathbf{D})$ (red region), b) fitting Gaussian on the posterior $p(\theta_t|\mathbf{D})$ (dark green), and c) kernel fitting on the posterior marginals (light green). (For interpretation of the references to color in this figure legend, the reader is referred to the web version of this article.)

trend and large variation for the FRF predictions. Finally, comparison to the Gaussian fit predictions indicates that this assumption also overestimates the prediction variability, showcasing again the importance of relying on the actual posterior and not on its Gaussian approximation at the MAP values. This comes at no surprise based on the results discussed earlier with respect to the expected poor approximation quality for Laplace's expansion.

In summary, the discussions above offer important insight with regard to Bayesian updating of PEH parameters using FRF observations. Significant correlation exists between some of the model characteristics leading to an unidentifiable problem in the MLE context, and therefore to a substantial influence of the prior knowledge, i.e. the assumed prior distributions, for the MAP identification. Nevertheless, if the intention is to improve the FRF predictability this has negligible impact as all approaches yield very good match to the experimental data, significantly improving in the application examined here the poor fit offered by the prior nominal model. For predicting posterior statistics of the FRF that extend beyond the mean FRF values, it was shown that the use of the actual posterior model parameter distribution instead of some form of approximation (point estimate approximation or reliance on marginal distributions only ignoring any correlations) is the preferred approach.

4.3. Model class selection

The Bayesian inference model class selection scheme is next adopted to examine different classes of models, all corresponding to the initial one, given by Eq. (15), simply with different number of uncertain characteristics that are updated using the observation data. A total of 5 models are considered, reviewed in Table 5, each with different number of uncertain variables. The first model (U_1) corresponds to the more complex model since all electromechanical properties and geomet-

rical parameters are considered as uncertain. For the remaining models the complexity is gradually decreased by reducing the number of characteristics considered as uncertain with the rest of the parameters considered as deterministic, having values and equal to their respective nominal values. The second model uses the nominal geometry, that is, it considers updating of only the PEH electromechanical properties, assuming that the geometry of the PEH can be measured with a high precision level. The third model considers only the parameters that exhibited significant trade-offs in the way they impact the FRF predictions, corresponding to the parameters that have moderate and high level of correlation, identified in red and yellow in Fig. 9. The fifth model further restricts this set to the parameters with high correlations, identified in red in Fig. 9. Finally, the fourth model considers only the characteristics that exhibited significant difference for the MAP values compared to the nominal ones. Note that each of the model classes is a subset of the previous one, apart from the pair U_3-U_4 since U_4 includes a parameter, $\varepsilon_{33}^T/\varepsilon_o$, that does not exist for U_3.

The MAP values associated with each model i are calculated and presented in Table 6. Due to space limitations only results for PEH-A model are presented here. Note that value of σ_e represents a measure of the data fit for each model class [22]. Some considerable variations (in range of 7–13%) are identified for the MAP values compared to the complete model U_1, with models U_1, U_2 and U_4 offering same fit to the observations (same σ_e values). It is evident that not including parameter $\varepsilon_{33}^T/\varepsilon_o$ reduces ability of models U_3 and U_5 to fit the data as well as the other three. Nevertheless, all models lead to MAP parameters that significantly differ from the nominal ones, indicating ability to extract information from the observed data to update the model description, and offer an improved fit to the observation data, as they all have σ_e values similar to model U_1, already shown to provide a very good match to the observations, especially when compared to the nominal model

Selection of the most appropriate model class needs to rely, though on the posterior probability given by Eq. (13), whose estimation entails calculation of the evidence $p(\hat{\mathbf{h}}|\hat{\mathbf{W}}, U_i)$. This evidence is calculated both via TMCMC as discussed in Section 2.2 and also by applying the Laplace's method of asymptotic approximation presented in Eq. (14). The posterior model probability is calculated assuming that all models are equally plausible based on our prior knowledge, leading to $P(U_i|\mathbf{D}, U) = 1/5$. Results are presented in Table 7 for both PEH devices. Both the posterior model probability and the log(evidence) (in parenthesis) are reported in this table. Note that since the prior is identical for all model classes, the log(evidence) is a scaled indicator of the posterior probability of each model. First of all, differences are observed between the two computational approaches for calculating the evidence, TMCM and Laplace's asymptotic expansion, with the first one yielding higher importance (based on posterior probability) for models U_1 and U_2 and the second for model U_4. Not surprisingly models U_3 and U_5 already identified to yield a poorer fit to the data (based on the σ_e values reported in Table 6) have practically zero preference based on the posterior model distributions as their log(evidence) is much smaller than the other models, independent of the computational approach adopted to calculate the evidence. The differences between TMCMC and Laplace's asymptotic expansion are not surprising, since as discussed in the previous section the accuracy of point estimate approximation of statistics is expected to be poor for the PEH application examined here. As such, the use of Laplace's

Table 5
Review of the five different model classes examined for model class selection. The distinction is imposed with respect to the number of model characteristics. In parenthesis next to each model the dimension of $\boldsymbol{\theta}$, n_θ, is reported.

Model	Parameters considered uncertain	Description
U_1 ($n_\theta = 12$)	All	Full set of model Parameters
U_2 ($n_\theta = 8$)	ζ, s_{11}^E, d_{31}, $\varepsilon_{33}^T/\varepsilon_o$,$\rho_s$,$\rho_p$,$E_s$,$\sigma_e$	All parameters except the geometrical characteristic
U_3 ($n_\theta = 6$)	ζ, s_{11}^E, d_{31},ρ_s,ρ_p,σ_e	Parameters with moderate or high correlation
U_4 ($n_\theta = 5$)	ζ, s_{11}^E, d_{31}, $\varepsilon_{33}^T/\varepsilon_o$,$\sigma_e$	Parameters with major differences between MAP and nominal values
U_5 ($n_\theta = 4$)	ζ, s_{11}^E, d_{31},σ_e	Parameters with the greatest correlation

Table 6
MAP values for PEH-A for the five examined model classes.

Model Parameter	Nominal	U_1	U_2	U_3	U_4	U_5
ρ_s[kg m^{-3}]	7400	7263	8233	9074	–	–
E_s[GN m^2]	61.0	62.7	61.6	–	–	–
s_{11}^E[pN^{-1} m^2]	16.40	18.25	18.69	17.87	19.63	19.64
$-d_{31}$ [pC N^{-1}]	320.0	261.4	265.4	245.0	278.9	269.2
$\varepsilon_{33}^T/\varepsilon_o$[F m^{-1}]	4500	8466	8830	–	8844	–
ρ_p[kg m^{-3}]	7400	7372	7541	7648	–	–
L [mm]	40.0	40.6	–	–	–	–
b [mm]	10.0	10.1	–	–	–	–
h_p[mm]	0.248	0.244	–	–	–	–
h_s[mm]	0.234	0.234	–	–	–	–
ζ	0.017	0.013	0.014	0.014	0.013	0.013
σ_e	0.1	0.0219	0.0219	0.0293	0.0219	0.0294

Table 7
Results of the model class selection performed for the two PEHs studied. The value of $P(M_i|\mathbf{D})$ for each model is presented together with its respective log-evidence (in parenthesis). Results obtained from both TMCMC and Laplace's approximation are reported.

Type	Method	U_1	U_2	U_3	U_4	U_5
PEH-A	TMCMC	0.323 (222.099)	0.638 (222.779)	0.000 (196.221)	0.039 (219.996)	0.000 (194.774)
	Laplace	0.000 (213.0155)	0.021 (221.8304)	0.000 (198.8461)	0.979 (225.6800)	0.000 (201.5678)
PEH-B	TMCMC	0.180 (293.6814)	0.816 (295.1884)	0.000 (169.6311)	0.004 (289.7453)	0.000 (168.2093)
	Laplace	0.000 (285.9100)	0.028 (291.8911)	0.000 (172.7758)	0.972 (295.4343)	0.000 (175.4139)

approximation can lead to erroneous results, as actually happens here, with preference shifting to model U_4 compared to the TMCMC case. Results from TMCMC have higher degree of confidence and therefore should be the ones used. These results show that model U_2 is the preferred one among the five considered, with model U_1 also showing a considerable degree of preference. In a model class averaging setting, both of these model classes could be utilized with weights given by the posterior probabilities $P(U_i|\mathbf{D}, U)$ in Table 7. If one model is only used, then that should be U_2. The preference for the less complicated model verifies also in this context that Bayesian model class selection automatically enforces the principle of model parsimony. Note that the small differences between models U_1 and U_2 can be also attributed to the fact that the prior probability models for the geometric characteristics have small coefficient of variation (see Table 1 earlier), leading to smaller differences between the model classes that differ only with respect to these characteristics.

4.4. Extension to consider the variability of the observations in the PEH identification

Finally, the extension to explicitly consider the variability of the experiments observations is discussed. This is performed only for PEH-B since as discussed earlier for PEH-A the variability in these observations is very small. Instead of using the mean over all experimental trials as the observation data, all observations are utilized here. Though as discussed earlier this can be accommodated in multiple ways, leading possibly to variations of the Bayesian updating framework discussed in Section 2, a simplified implementation is considered here by modifying the likelihood function to explicitly consider all observations. For the multiplicative prediction error, which has been our focus here, this likelihood function is transformed to

$$p\left(\hat{\mathbf{h}}\middle|\theta_t, \hat{\mathbf{W}}\right) = \left(\frac{1}{\sigma_e\sqrt{2\pi}}\right)^{N_e M}\left(\prod_{s=1}^{N_e}\prod_{m=1}^{M}\frac{1}{\hat{h}_{m,s}}\right)\exp\left[-\frac{1}{2\sigma_e^2}\sum_{m=1}^{M}\sum_{s=1}^{N_e}\left(\ln\left[\hat{h}_{m,s}\right] - \ln[H(\theta,\hat{\omega}_m)]\right)^2\right] \tag{20}$$

where N_e is the total number the FRF experimental identification was repeated (20 in this case) and $\hat{h}_{m,s}$ is the measured FRF value for frequency $\hat{\omega}_m$ for the s-th experimental trial. The Bayesian identification scheme is then repeated using this new likelihood function. The impact of the observation variability on this scheme is demonstrated using the predicted FRF. Note that illustrating this impact with respect to the identified model parameters poses a significant challenge for the PEH application due to the aforementioned trade off in the way these parameters impact the FRF response: the variability in the identified model parameters stems from both the variability in the observations as well from this trade-off. This is also why emphasis on the implementation of the Bayesian scheme was placed on using the mean observations (across the experimental trials) instead of all the observations. This approach allowed us to decouple the sources of the observed variability on the model parameters and offer a critical assessment of the characteristics related to model identifiability for this application.

Fig. 11 shows the predicted mean FRF (solid line) along with its variability corresponding to ±three standard deviation (dashed line) using samples from the posterior PDF obtained through TMCMC for the cases that all the observations (red

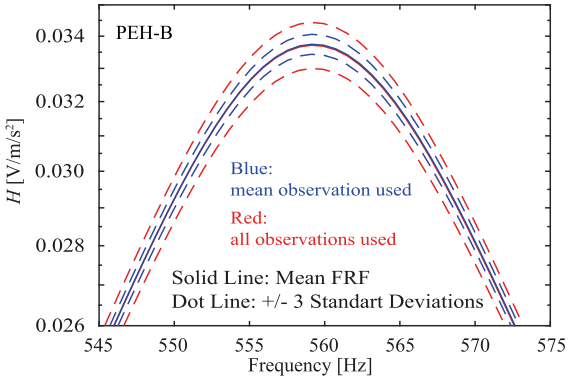

Fig. 11. Mean FRF along with variability corresponding to ±3 standard deviations for PEH-B for the cases that all the observations or the observation mean are used for each frequency as experimental data. The statistics for the FRF curve are calculated using TMCMC samples.

curves) or the observation mean (blue line) are used for each frequency. Figure is zoomed in around the peak of the FRF function to better illustrate the differences between the two cases. It is evident that the mean predictions are identical but the variability of these predictions increases when all observations are utilized as experimental data. Still even in that case the predicted variability is small. This should be attributed to the fact that the coefficient of variation for the observations is, as discussed earlier, small. Comparison demonstrates though that for capturing better the uncertainties introduced in the problem from the experimental setup it might be necessary to explicitly consider all experimental trials, especially if the observation variability is large, since they have an effect on the higher order statistics of the predicted FRF, and subsequently on any decisions made using FRF statistics beyond the mean predictions.

5. Conclusions

This study examined the implementation of a Bayesian model updating framework for estimating the electromechanical properties of PEHs using experimental FRF observations. The Bayesian inference framework was reviewed for updating the PEH model properties including quantification of the variability of these properties (posterior distribution updating), facilitating predictions using the updated model properties (posterior predictive analysis) and evaluating appropriateness of different candidate models (model class selection). Two different computational approaches were discussed for approximating statistics for the updated model: using point estimate methods relying on the MAP (or MLE) parameters or utilizing samples from the posterior distribution obtained by TMCMC. It was shown that the overall framework enjoys a series of advantages for PEH applications as: (1) it is compatible with any deterministic predictor of the PEH response, (2) it identifies both the most probable values of the electromechanical properties as well as the probable space these properties lie in, (3) it quantifies the confidence interval for the predicted FRF, and (4) it can be further used to select the most adequate model if different predictive models are available.

Implementation of this framework was considered for two commercial bimorph cantilevered piezoelectric harvesters, each of them with identical nominal electromechanical characteristics but having different geometries. The adopted predictive FRF model corresponds to a standard modal expansion approach. Two different model prediction errors were examined: an additive and a multiplicative error. It was observed that both approaches lead to the same MAP values, though a strong preference was recommended for the multiplicative prediction error as it leads to predictive FRF with coefficient of variation independent of the frequency. It was shown that the likelihood function is not globally identifiable, having multiple global minima, indicating a significant trade-off between the different electromechanical properties. In other words, there is not a unique set of electromechanical parameters that match the experimental results. The MAP estimation yields a globally identifiable problem, though preference in this instance is evidently influenced by the prior knowledge, which dictates which of the candidate minima for the likelihood function is ultimately selected. Any differences between the MAP and MLE values do not translate to differences for the estimated FRF. Samples from the posterior, obtained through TMCMC, demonstrated considerable variability showing that the posterior PDF is not significantly peaked. Also it was shown that this posterior cannot be approximated by a Gaussian distribution. These features indicate that approximate methods (leveraging Laplace's expansion) are not recommended for estimating higher order posterior statistics of the FRF, such as variance or model evidence. Comparison between different approximate methods to capture the FRF variability showed that only an approach that uses the exact samples from the posterior distribution can accurately capture this variability. Implementation of Bayesian model class selection demonstrated how the principle of model parsimony can be naturally enforced, in this application identifying the model that considers only the electromechanical properties as uncertain (and fixing the geometrical properties to their nominal values) as the most appropriate one. Overall the presented framework should be regarded as a powerful tool for robust design/prediction or the identification of properties for piezoelectric energy harvesters.

Declaration of Competing Interest

The authors declare that they have no known competing financial interests or personal relationships that could have appeared to influence the work reported in this paper.

Acknowledgments

This research was supported by the Chilean National Fund for Scientific and Technological Development (FONDECYT) (grant 11180812) and the Vice Presidency of Research and Development (VID) at Universidad de Chile (Support for Research, Innovation and Artistic Creation Events 2018).

Appendix A TMCMC overview

TMCMC [34] relies on a sequential implementation, using samples from density $p_j(\theta_t|\mathbf{D})$ to obtain samples from density $p_{j+1}(\theta_t|\mathbf{D})$. The process of obtaining N_s such samples is:

Step 1: Based on the N_s available samples $\{\theta_t\}_j = \left\{\theta^1_{t(j)}, \ldots, \theta^{N_s}_{t(j)}\right\}$ from the precedent intermediate distribution $p_j(\theta_t|\mathbf{D})$, the transition coefficient q_{j+1} is chosen such that the sample-based coefficient of variation (COV) of the quantity $p_{j+1}(\theta_t|\mathbf{D})/p_j(\theta_t|\mathbf{D}) = p(\hat{\mathbf{h}}\big|\,\theta_t, \hat{\mathbf{W}})^{q_{j+1}-q_j}$ equals to a set value, typically 100%. The sample weights are then calculated proportional to the quotient of the two densities:

$$w_{j+1}(\theta) = p_{j+1}(\theta_t|\mathbf{D})/p_j(\theta_t|\mathbf{D}) = p(\hat{\mathbf{h}}|\,\theta_t, \mathbf{W})^{q_{j+1}-q_j} \tag{21}$$

This leads to the mean of the weights

$$\hat{S}_{j+1} = \frac{1}{N_s}\sum_{p=1}^{N_s} w_{j+1}(\theta^p_{t(j)}) \tag{22}$$

and to weighted sample mean and covariance matrix:

$$\begin{aligned}\bar{\theta}_{j+1} &= \tfrac{1}{N_s\hat{S}_{j+1}}\sum_{p=1}^{N_s}\left[w_{j+1}(\theta^p_{t(j)})\theta^p_{t(j)}\right]\\ \Sigma_{j+1} &= \tfrac{1}{N_s\hat{S}_{j+1}}\sum_{p=1}^{N_s}\left[w_{j+1}(\theta^p_{t(j)})(\theta^p_{t(j)}-\bar{\theta}_{j+1})(\theta^p_{t(j)}-\bar{\theta}_{j+1})^T\right]\end{aligned} \tag{23}$$

Step 2: Re-sample N_t samples $\{\boldsymbol{\theta}_t\}_l = \{\boldsymbol{\theta}^1_{t(l)}, \ldots, \boldsymbol{\theta}^{N_t}_{t(l)}\}$ with replacement from the set $\{\theta_t\}_j$ according to their weights w_{j+1}. These ultimately correspond to samples from $p_{j+1}(\theta_t|\mathbf{D})$. After this resampling stage, which is implemented for each of the intermediate densities, initialize independent Markov chains from each of these samples. For each chain ($c = 1, \ldots, N_t$), repeat random walk Markov moves using step $\beta^2\Sigma_{j+1}$ where β is a scaling factor which is suggested to be set to 0.2 [34]. Specifically, the p^{th} random walk move in the c^{th} chain to simulate sample $\theta^p_{t(c)}$, is performed as follows: (a) simulate a candidate sample $\tilde{\theta}^p_{t(c)}$ from a Gaussian distribution with mean $\theta^{p-1}_{t(c)}$ and covariance $\beta^2\Sigma_{j+1}$ and u from uniform [0,1]; (b) set $\theta^p_{t(c)} = \tilde{\theta}^p_{t(c)}$ if the following condition is met:

$$\frac{p_{j+1}\left(\tilde{\theta}^p_{t(c)}\middle|\mathbf{D}\right)p\left(\tilde{\theta}^p_{t(c)}\right)}{p_{j+1}\left(\theta^{p-1}_{t(c)}\middle|\mathbf{D}\right)p\left(\theta^{p-1}_{t(c)}\right)} \geqslant u \tag{24}$$

otherwise set $\theta^p_{t(c)} = \theta^{p-1}_{t(c)}$. Note that for the cth chain the initial seed θ^0_c is the cth element of set $\{\theta_t\}_l$. After completing total of N_s Markov random walk moves for all chains combine the samples to obtain sample set $\{\theta_t\}_{j+1} = \left\{\theta^1_{t(j+1)}, \ldots, \theta^{N_s}_{t(j+1)}\right\}$ from the intermediate distribution $p_{j+1}(\theta_t|\mathbf{D})$.

Appendix B. Supplementary data

Supplementary data to this article can be found online at https://doi.org/10.1016/j.ymssp.2019.106506.

References

[1] A. Erturk, D.J. Inman, A distributed parameter electromechanical model for cantilevered piezoelectric energy harvesters, J. Vib. Acoust. Trans. ASME 130 (4) (2008).
[2] A. Erturk, D.J. Inman, On mechanical modeling of cantilevered piezoelectric vibration energy harvesters, J. Intell. Mater. Syst. Struct. 19 (11) (2008) 1311–1325.
[3] A. Erturk, D.J. Inman, An experimentally validated bimorph cantilever model for piezoelectric energy harvesting from base excitations, Smart Mater. Struct. 18 (2) (2009) 025009.
[4] C.D.M. Junior, A. Erturk, D.J. Inman, An electromechanical finite element model for piezoelectric energy harvester plates, J. Sound Vib. 327 (1) (2009) 9–25.
[5] U. Von Wagner, P. Hagedorn, Piezo–beam systems subjected to weak electric field: experiments and modelling of non-linearities, J. Sound Vib. 256 (5) (2002) 861–872.
[6] S.C. Stanton, A. Erturk, B.P. Mann, E.H. Dowell, D.J. Inman, Nonlinear nonconservative behavior and modeling of piezoelectric energy harvesters including proof mass effects, J. Intell. Mater. Syst. Struct. 23 (2) (2012) 183–199.
[7] A. Abdelkefi, A. Nayfeh, M. Hajj, Global nonlinear distributed-parameter model of parametrically excited piezoelectric energy harvesters, Nonlinear Dyn. 67 (2) (2012) 1147–1160.
[8] S. Leadenham, A. Erturk, Unified nonlinear electroelastic dynamics of a bimorph piezoelectric cantilever for energy harvesting, sensing, and actuation, Nonlinear Dyn. 79 (3) (2015) 1727–1743.
[9] M. Akbar, J.L. Curiel-Sosa, Evaluation of piezoelectric energy harvester under dynamic bending by means of hybrid mathematical/isogeometric analysis, Int. J. Mech. Mater. Des. (2017) 1–21.
[10] M. Kim, M. Hoegen, J. Dugundji, B.L. Wardle, Modeling and experimental verification of proof mass effects on vibration energy harvester performance, Smart Mater. Struct. 19 (4) (2010) 045023.

[11] R.O. Ruiz, V. Meruane, Uncertainties propagation and global sensitivity analysis of the frequency response function of piezoelectric energy harvesters, Smart Mater. Struct. 26 (6) (2017) 065003.
[12] P. Peralta, R.O. Ruiz, V. Meruane, Experimental study of the variations in the electromechanical properties of piezoelectric energy harvesters and their impact on the frequency response function, Mech. Syst. Signal Process. 115 (2019) 469–482.
[13] T.C. de Godoy, M.A. Trindade, Effect of parametric uncertainties on the performance of a piezoelectric energy harvesting device, J. Braz. Soc. Mech. Sci. Eng. 34 (SPE2) (2012) 552–560.
[14] V.R. Franco, P.S. Varoto, Parameter uncertainties in the design and optimization of cantilever piezoelectric energy harvesters, Mech. Syst. Signal Process. 93 (2017) 593–609.
[15] S. Gurav et al., "Uncertainty-based design optimization of a micro piezoelectric composite energy reclamation device," in 10th AIAA/ISSMO Multidisciplinary Analysis and Optimization Conference, 2004, p. 4619.
[16] S.F. Ali, M.I. Friswell, S. Adhikari, Piezoelectric energy harvesting with parametric uncertainty, Smart Mater. Struct. 19 (10) (2010) 105010.
[17] A.H. Hosseinloo, K. Turitsyn, Design of vibratory energy harvesters under stochastic parametric uncertainty: a new optimization philosophy, Smart Mater. Struct. 25 (5) (2016) 055023.
[18] S. Seong, C. Hu, S. Lee, Design under uncertainty for reliable power generation of piezoelectric energy harvester, J. Intell. Mater. Syst. Struct. 28 (17) (2017) 2437–2449.
[19] L. Ljung, System identification, in: Signal analysis and Prediction, Springer, 1998, pp. 163–173.
[20] A. Gelman, H.S. Stern, J.B. Carlin, D.B. Dunson, A. Vehtari, D.B. Rubin, Bayesian Data Analysis, Chapman and Hall/CRC, 2013.
[21] J.L. Beck, Bayesian system identification based on probability logic, Struct. Control Health Monit. 17 (7) (2010) 825–847.
[22] J.L. Beck, A.A. Taflanidis, Prior and posterior robust stochastic predictions for dynamical systems using probability logic, Int. J. Uncertain. Quantif. 3 (4) (2013) 271–288.
[23] C. Papadimitriou, J.L. Beck, L.S. Katafygiotis, Updating robust reliability using structural test data, Probabilistic Eng. Mech. 16 (2) (2001) 103–113.
[24] G. Cowan, Statistical Data Analysis, Oxford University Press, 1998.
[25] L. Wang, X. Wang, Y. Li, J. Hu, A non-probabilistic time-variant reliable control method for structural vibration suppression problems with interval uncertainties, Mech. Syst. Signal Process. 115 (2019) 301–322.
[26] L. Wang, C. Xiong, X. Wang, Y. Li, M. Xu, Hybrid time-variant reliability estimation for active control structures under aleatory and epistemic uncertainties, J. Sound Vib. 419 (2018) 469–492.
[27] L. Wang, X. Wang, Y. Li, G. Lin, Z. Qiu, Structural time-dependent reliability assessment of the vibration active control system with unknown-but-bounded uncertainties, Struct. Control Health Monit. 24 (10) (2017) e1965.
[28] M. Faes et al, A multivariate interval approach for inverse uncertainty quantification with limited experimental data, Mech. Syst. Signal Process. 118 (2019) 534–548.
[29] P.E. Hadjidoukas, P. Angelikopoulos, C. Papadimitriou, P. Koumoutsakos, Pi 4U: a high performance computing framework for Bayesian uncertainty quantification of complex models, J. Comput. Phys. 284 (Mar. 2015) 1–21.
[30] K.-V. Yuen, Bayesian Methods for Structural Dynamics and Civil Engineering, John Wiley & Sons, 2010.
[31] S.H. Cheung, J.L. Beck, Calculation of posterior probabilities for Bayesian model class assessment and averaging from posterior samples based on dynamic system data, Comput. Civ. Infrastruct. Eng. 25 (5) (2010) 304–321.
[32] C. Papadimitriou, J. L. Beck, and L. S. Katafygiotis, "Asymptotic expansions for reliabilities and moments of uncertain dynamic systems," 1995.
[33] S.K. Au, C. Papadimitriou, J.L. Beck, Reliability of uncertain dynamical systems with multiple design points, Struct. Saf. 21 (2) (1999) 113–133.
[34] J. Ching, Y.-C. Chen, Transitional Markov chain Monte Carlo method for Bayesian model updating, model class selection, and model averaging, J. Eng. Mech. 133 (7) (2007) 816–832.
[35] W. Betz, I. Papaioannou, D. Straub, Transitional markov chain monte carlo: observations and improvements, J. Eng. Mech. 142 (5) (2016) 04016016.
[36] S. He, C.-T. Ng, Guided wave-based identification of multiple cracks in beams using a Bayesian approach, Mech. Syst. Signal Process. 84 (2017) 324–345.
[37] R. Rocchetta, M. Broggi, Q. Huchet, E. Patelli, On-line Bayesian model updating for structural health monitoring, Mech. Syst. Signal Process. 103 (2018) 174–195.
[38] M. Muto, J.L. Beck, Bayesian updating and model class selection for hysteretic structural models using stochastic simulation, J. Vib. Control 14 (1–2) (2008) 7–34.
[39] R.M. Neal, Annealed importance sampling, Stat. Comput. 11 (2) (2001) 125–139.
[40] L. Martino, V. Elvira, and D. Luengo, "Anti-tempered layered adaptive importance sampling," in 2017 22nd International Conference on Digital Signal Processing (DSP), 2017, pp. 1–5.
[41] L. Martino, V. Elvira, D. Luengo, J. Corander, Layered adaptive importance sampling, Stat. Comput. 27 (3) (2017) 599–623.
[42] E. Marinari, G. Parisi, Simulated tempering: a new Monte Carlo scheme, EPL Europhys. Lett. 19 (6) (1992) 451.
[43] X. Yuan, Z. Lu, C. Zhou, Z. Yue, A novel adaptive importance sampling algorithm based on Markov chain and low-discrepancy sequence, Aerosp. Sci. Technol. 29 (1) (2013) 253–261.
[44] A. Erturk, D.J. Inman, Piezoelectric energy harvesting, John Wiley & Sons, 2011, John Wiley & Sons, 2011.
[45] R.D. Rosenkrantz, E.T. Jaynes, Papers on Probability, Statistics and Statistical Physics vol. 158 (2012) 158.
[46] H.-P. Wan, W.-X. Ren, Stochastic model updating utilizing Bayesian approach and Gaussian process model, Mech. Syst. Signal Process. 70 (2016) 245–268.
[47] E. Simoen, C. Papadimitriou, G. Lombaert, On prediction error correlation in Bayesian model updating, J. Sound Vib. 332 (18) (2013) 4136–4152.
[48] L.D. Lutes, S. Sarkani, Stochastic analisys of structural and mechanical vibrations, Prentice Hall, 1997.
[49] "Sinocera," http://www.sinocera.net/, 2016.